JOURNAL OF APPLIED ELECTROCHEMISTRY 13 (1983) 743–750

Photoelectrochemical reactions of FeS_2 (pyrite) with H_2O and reducing agents

W. JAEGERMANN, H. TRIBUTSCH

Hahn-Meitner-Institut für Kernforschung Berlin GmbH, Bereich Strahlenchemie, D-1000 Berlin 39, Postbox, Federal Republic of Germany

Received 20 January 1983

The photoelectrochemical behaviour of natural and synthetic FeS_2 (pyrite) has been investigated. In all cases anodic photocurrents have been observed. From photocurrent spectra an energy band gap of 0.9 eV has been determined. The reaction of photogenerated holes produced on d-states of the Fe^{2+} ions with water leads to the formation of SO_4^{2-} as a corrosion product. This is contrary to the photoreaction of RuS_2 with H_2O which yields oxygen, although the crystal as well as the electronic structure of both compounds is equivalent. The differences are discussed in terms of the transition metal chemistry of iron and ruthenium, respectively. Like with other d-band semiconductors a shift of the onset of photocurrents with the redox potential of electron donors has been observed. This study is part of systematic investigations of catalytic requirements for the photoelectrolysis of water.

1. Introduction

Transition metal chalcogenides have been shown to be promising semiconductors for electrochemical regenerative as well as photoelectrolysis cells [1, 2]. They show remarkable stability against anodic photocorrosion if their valence band can be derived from metal d-states (n-type semiconductor).

With some metal chalcogenides it is possible to oxidize H_2O producing O_2 at the semiconductor anode, whereas with others only corrosion to XO_4^{2-} (X = S, Se, Te) has been observed when no additional redox couples are present. For example with PtS_2 the photoassisted oxidation of H_2O to O_2 is possible [3] whereas the MX_2 semiconductors with M = Mo, W, and X = S, Se, Te corrode heavily in the absence of redox couples, in spite of crystallizing in a similar layered type structure [1, 2, 4].

As very promising material RuS_2 has been tested for the photoassisted oxidation of H_2O showing very high quantum yields as single crystal and no detectable side reactions [5, 6]. For an understanding of the influence of the metal on the reaction pathways, we considered it worthwhile to study the photoelectrochemical behaviour of FeS_2 (pyrite) having the same crystal as well as electronic structure as RuS_2.

Both compounds crystallize in a cubic structure (space group *Pa*3) as NaCl with the anion sites occupied by S_2^{2-} ions. The S–S distances in FeS_2 are 218 pm and the Fe–Fe distances 381 pm [7], thus excluding strong metal–metal interactions. Each iron atom is octahedrally coordinated by sulphur (with slight deviations) with an average Fe–S bond length of 226 ppm.

The strong octahedral crystal field of the S_2^{2-} ions removes the degeneracy of the d-orbitals resulting in a $t_{2g}^6 e_g^0$ configuration for the Fe^{2+} as is suggested by the diamagnetism of FeS_2 [8, 9]. The band structure is given in Fig. 1. A very broad band mainly of sulphur 3p character is superposed by a narrow band derived from the metal t_{2g} levels. The empty conduction band has mainly iron e_g character with some sulphur 3p mixing [8, 10–12].

This band model, which is also valid for RuS_2 [13, 14], can be used to interpret the electric, magnetic, and optical properties of solids with pyrite type structure. The optical transitions across the band gap (~ 1.8 eV for RuS_2 and 0.9 eV for FeS_2) occur between nearly nonbonding bands derived from the metal d-levels. Therefore the photogenerated holes, which arrive at the surface

0021-891X/83 $03.00 + .12

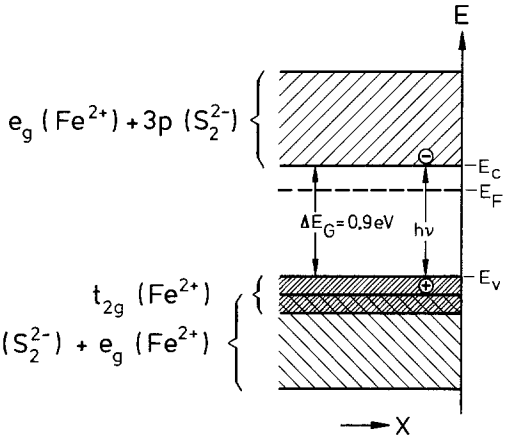

Fig. 1. Schematic band energy diagram for FeS_2 (pyrite).

on d-states, produce strongly interacting (chemisorbed) intermediates thus decreasing the energy requirement for the water oxidation reaction. Differences in the reaction pathways can directly be attributed to different catalytic effectivity of the different metals.

2. Experimental details

The pyrite used in the experiments were from different natural sources. For comparison, synthetic FeS_2 grown by vapour transport has also been tested. The results obtained were identical in all cases. The crystals were cut into slices with a thickness of approximately 1 mm along the planes of the cubic lattice with surface areas between 10 and 40 mm^2. The surfaces were etched for 10 min with a mixture of 10 cm^3 H_2O_2 solution (30%), 10 cm^3 hydrochloric acid (38%) and 20 cm^3 H_2O (alternatively aqua regia) to remove the residues of the cutting procedure. These cleaned surfaces show the same photochemical behaviour as the natural untreated areas.

The ohmic back contact was made with indium–mercury alloy. The crystals were fixed by silver paste (3M) onto an electrode holder of teflon (Vespel). The sides of the crystals and the brass centre of the electrode holder were isolated with epoxy (3M). As light sources either a 450 W Xe-lamp (Oriel) or a 240 W W-lamp (Oriel) were used and the photocurrent spectra were obtained with a monochromator (Oriel) equipped with either a 500 nm or 1 μm blazed grating.

Electrochemical studies were performed in a closed electrochemical cell with purging by nitrogen. The standard three electrode arrangement was used with a platinum electrode as counter and a saturated calomel electrode (Metrohm) as reference electrode, respectively. All potentials are given with respect to the SCE. Cyclic voltammograms were measured with a potentiostat (PAR 173) coupled to a scan generator (PAR 175). In order to separate the large dark currents from the photocurrent the light was modulated with a chopper (PAR 9479) and the photocurrent was detected with a lock-in amplifier (PAR 124A).

The ESCA spectra were recorded with a commercial electron spectrometer system (VG ESCALAB MK I) providing a pressure of better than 5×10^{-8} mbar during the measurements. The specimens were fixed with silver paste to the specimen holders. The resolution (MgK_λ line) was 1.5 eV (Ag 3 $d_{5/2}$ peak). The spectra were calibrated against C 1 $s_{1/2}$ = 285.0 eV.

3. Experimental results

The electrochemical behaviour of FeS_2 in the dark is similar to that of a metal. No blocking of currents can be observed as should be expected for a good semiconductor-electrolyte junction. This property and the low resistivity $< 1\ \Omega\,cm^{-1}$ [15] indicates a high doping level of natural pyrite.

In alkaline medium (Fig. 2) and during the sweep to negative potential, the reduction of the S_2^{2-} ions in the lattice occurs (E_0 (S_2^{2-}/S^{2-}) = -0.76 V [16]) before the evolution of H_2 begins at -1.4 V. At this cathodic polarization a black film, probably FES, is formed on the surface and the smell of H_2S can be noticed. In acidic medium the onset of hydrogen production at -0.50 V is followed by a chemical reduction of FeS_2 leading also to FeS [17–20].

At positive polarization a corrosion reaction to SO_4^{2-} and Fe^{3+} appears [19, 20], and a reddish brown film is formed, probably containing hydrous Fe(III)-oxide [21]. No oxidation of H_2O to O_2 could be observed.

In spite of the quasi-metallic behaviour of the FeS_2 electrode, photoeffects can easily be detected with the aid of lock-in amplifier technique (Fig. 3). All FeS_2 specimens investigated showed the behaviour of a n-type semiconductor with anodic photocurrents. In alkaline medium, the

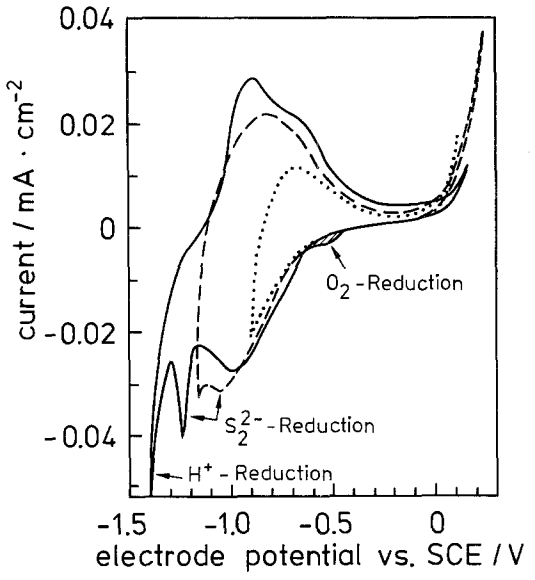

Fig. 2. Cyclic voltammograms of FeS_2 electrodes in 0.1 mol dm^{-3} NaOH (Scan speed: 10 mV s^{-1}). The reduction peak of O_2 is only present when purging with nitrogen is not applied.

photocurrent decreases to zero at − 0.9 V (vs SCE) with a strong hysteresis exhibiting lower photocurrents in the sweep towards positive potentials. This hysteresis is also present if the potential does not reach the photocurrent onset potential (e.g. in acidic medium). Whereas negative polarization destroys the photoeffects by forming the black film, no strong influence of polarization to positive potentials was detected. At higher positive voltages the photocurrent does not increase much beyond the value observed between − 0.5 and + 0.5 V.

The photocurrent responses to rectangular light pulses at different potentials are included in Fig. 3 showing the different kinetics in these potential regions. At − 0.67 V the rectangular anodic photoresponse indicates that the oxidation reaction is not inhibited during the time scale of the experiments (10 to 100 ms). Probably the reduction of S_2^{2-} by the dark current is reversed again by the light driven oxidation. This assumption of a back reaction is also supported by the photocurrent–time curve at this potential (Fig. 4) showing only a rather small decrease of photocurrent even when a charge corresponding to 6000 monolayers has been passed. An oxidation of S_2^{2-} to elemental sulphur cannot be noticed either.

At more positive potentials the photocurrent response exhibits spikes typical for an oxidation process to some intermediate, where the following steps are rather slow, which is followed by a back reaction (reduction) in the dark. When the potential range of the anodic dark current is reached, the photoresponse curves change to more rectangular shapes again. These photocurrent transients reflect the mechanisms of formation of an intermediate and of the end product of the corrosion process, respectively.

The spectral dependence of the photocurrent is displayed in Fig. 5. The variation of the imaginary part k of the complex refractive index with the wavelength obtained by reflectance spectra [8], has been inserted. The agreement for the bandgap of a value of 0.9 eV measured in photocurrent

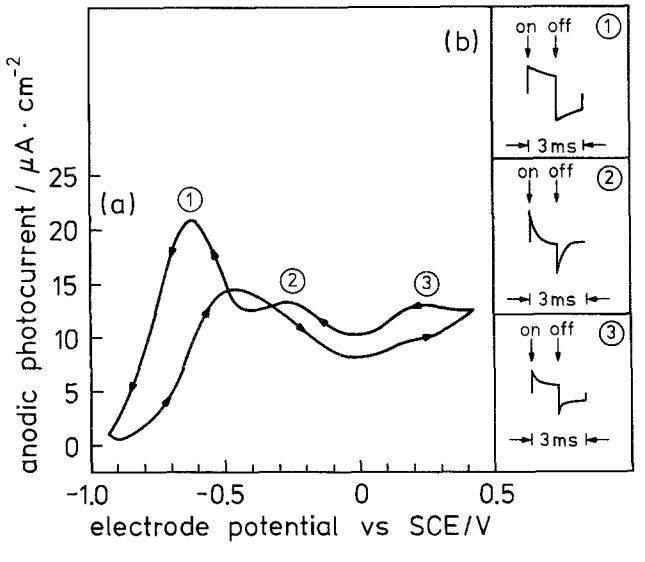

Fig. 3. (a) Photocurrent-potential curve of FeS_2 in 0.1 mol dm^{-3} NaOH (Scan speed: 10 mV s^{-1}). (b) Inserted pictures show the photocurrent-time transients at different applied potentials.

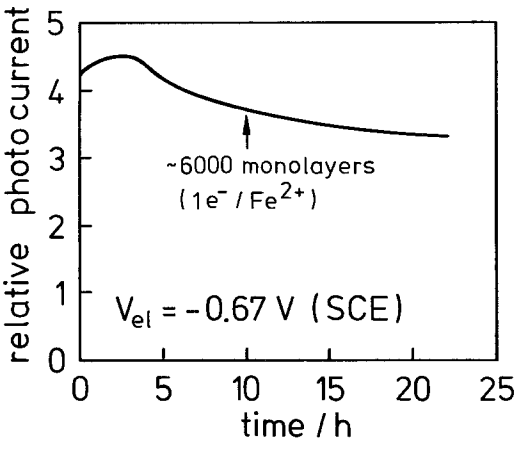

Fig. 4. Anodic photocurrent dependence on time. The point, where a charge corresponding 6000 monolayers assuming the reaction $Fe^{2+} + h \rightarrow Fe^{3+}$ has been passed, is indicated.

spectra with the data from the optical measurement is reasonably good. The structures in the photocurrent spectra have been obtained with several independent FeS_2-crystals, although their origin is not yet clear; in the optical spectra only weakly pronounced shoulders can be recognized [8].

The addition of different redox couples to the solution increases the measured photocurrents, e.g. by a factor of 10 for V^{2+}/V^{3+}. In all cases the photocurrent maxima can qualitatively be related to the redox potential of the redox couple (Fig. 6)

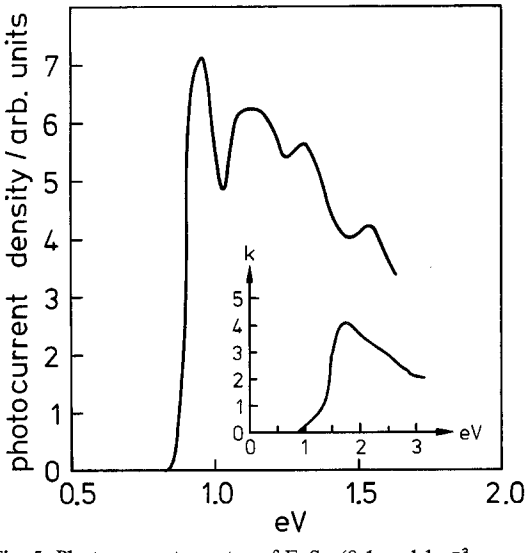

Fig. 5. Photocurrent spectra of FeS_2 (0.1 mol dm^{-3} NaOH, -0.67 V vs SCE). The inserted curve shows the complex refractive index as function of photon energy.

as already shown for a number of other transition metal semiconductors with d-state valence bands [1, 3]. In the case of FeS_2, beyond the maximum a subsequent decrease of the photocurrents is observed with most redox couples (except for I_2/I^-) and it is correlated with a strong increase of the dark current originating from the oxidation wave at the non rectifying FeS_2 electrode.

The determination of the flat-band potential of FeS_2 by capacity measurements has been attempted. The capacity–voltage curves could not be analysed in the form of a Mott–Schottky plot, assuming just a series resistor/capacitor equivalent circuit. Probably the non ideal limiting behaviour of the samples resulting from high concentrations of impurities and/or crystal defects is responsible for this behaviour. During the capacity measurements a pronounced shift of phase with potential was observed.

4. Discussion

The most striking difference in the photoelectrochemical behaviour of FeS_2 compared to RuS_2 in aqueous electrolytes is the difference in the reaction pathways of the holes reaching the surface. Whereas with RuS_2 the oxidation of H_2O to O_2 takes place without a significant corrosion reaction even in the case of polycrystalline material [5, 6], FeS_2 exhibits only corrosion without detectable O_2 evolution. As the crystal structure and electronic configuration of the two compounds are similar, the reaction pathway is determined by the different influence of the metal on the reaction products or their intermediates. From the chemistry of ruthenium it is known that high oxidation states can easily be reached in contrast to iron of which only Fe^{II} and Fe^{III} are reasonable stable [23]. As the metal atoms on the surfaces are far apart (d(Fe–Fe) = 381 pm, d(Ru–Ru) = 396 pm [7, 24]) they cannot easily cooperate in the oxidation reaction of H_2O which needs a transfer of 4 holes. Therefore the high oxidation states (collection of several holes) on the metal which also have been found for the oxygen evolving metallic oxidation catalysts ruthenium and RuO_2 [25, 26] are only possible with RuS_2, whereas in FeS_2 oxidation of the S_2^{2-} groups will take place leading to a corrosion to SO_4^{2-} and Fe^{3+}.

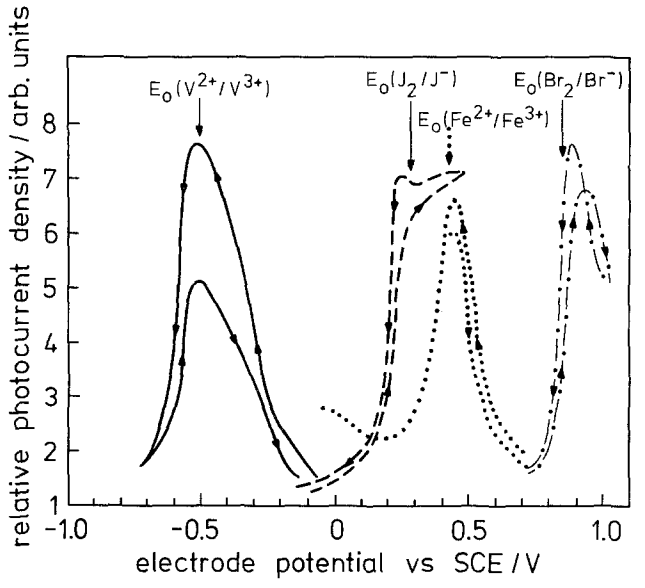

Fig. 6. Photocurrent-voltage curves for different redox couples (—— 0.5 mol dm^{-3} V^{2+}/V^{3+} in 5 mol dm^{-3} HCl [22], ———— 0.05 mol dm^{-3} I_2, 1 mol dm^{-3} KI in 0.1 mol dm^{-3} H_2SO_4, ... 0.1 mol dm^{-3} Fe^{2+}/Fe^{3+} in 0.1 mol dm^{-3} H_2SO_4, -.-.-. 1 mol dm^{-3} KBr in 0.1 mol dm^{-3} H_2SO_4).

In this context it is interesting to compare the XP-spectra of RuS_2 and FeS_2 crystals (Fig. 7). Whereas in RuS_2 the ruthenium and sulphur binding energies can be attributed to the simple ionic formula $Ru^{4+}S_2^{2-}$, in FeS_2 the sulphur peak is split into one signal, which can be assigned to the S_2^{2-} ion and a second one at higher binding energies, which can be related to oxidized sulphur (Table 1). The oxidized sulphur species on the surface of FeS_2 is present on the etched samples as well as on the natural areas. In addition the iron $2p_{3/2}$ signal shows besides the peak of FeS_2 some contribution of iron oxides at higher binding energies.

Moreover, the interaction of the metal with the possible intermediates O_2^{2-} or O_2^- of the water oxidation reaction is quite different for ruthenium and iron, as is known from the coordination chemistry of dioxygen species [30]. Whereas for ruthenium only complexes with a peroxo ligand (O_2^{2-}) coordinated side on to one single metal centre according to structure type I are known, iron forms dinuclear complexes with bridging O_2^{2-} groups (structure type II), and end on superoxo complexes (O_2^--ligands, structure type III) if the metal centres are too far away for cooperative bonding of one O_2^{n-} unit.

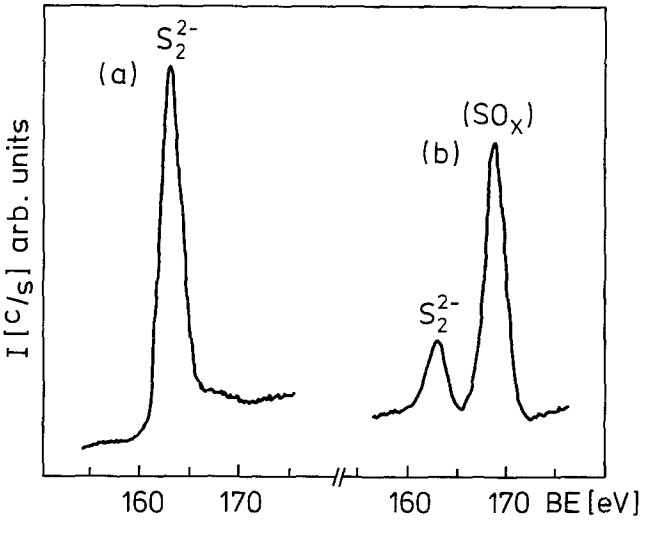

Fig. 7. XP-Spectra of RuS_2 (a) and FeS_2 (b) in the S 2p binding energy range.

Table 1. Binding energies of RuS_2, FeS_2, and similar compounds (Calibrated to C 1 $s_{1/2}$ = 285.0 eV)

	S 2 $s_{1/2}$	S 2p	Ru 3$d_{5/2}$	Fe 2$p_{3/2}$	*Reference*
RuS_2	227.0	163.2	280.5	–	–
Ru	–	–	278.8	–	27
RuO_2	–	–	282.8	–	27
FeS_2 ‡	227.0 (233.4)*	162.8 (169.4)*	–	~ 707 (~ 709, ~ 711)†	–
Fe	–	–	–	706.1	28
Fe_2O_3	–	–	–	711.5	27
Na_2S	–	162.0	–	–	27
S_8	–	164.2	–	–	27
S_2^2-complexes	–	163.4 §	–	–	29
Na_2SO_3	–	166.7	–	–	27
Na_2SO_4	–	168.9	–	–	27

* Oxidized S (SO_x) at the surface.
† Oxidized FeS_2 (FeO, Fe_2O_3) at the surface.
‡ For clean surfaces see [12].
§ Mean value.

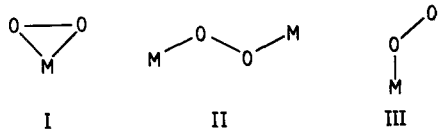

I II III

More detailed information on the intermediates and kinetics as well as on the semiconductor surface is necessary to understand the influence of the metal ions on the reaction path of the photogenerated holes completely.

Another interesting phenomenon which can usually be observed for transition metal sulphide semiconductors is the shift of the flat-band potentials [1, 3], caused by a high number of surface states or interbandgap states [31]. In addition to this shifting of the photocurrent with the redox potentials of the electron donor for FeS_2 electrodes, a rapid decrease of photocurrent appears when the potential exceeds the redox potential leading to a pronounced peak with a maximum nearly at the normal potential of the oxidation–reduction coupling (Fig. 7). This photocurrent potential dependence can be explained by an electronic scheme for the transfer mechanism of photogenerated charges. For this electronic scheme it is assumed that the band edges are not fixed at the surface, but are shifted parallel to the bulk band shift and that the depletion layer is rather thin. (For convenience it is assumed that the potential drop will only occur through the Helmholtz layer leaving the band bending uneffected which is certainly not the case in reality. But it is not easy to evaluate the relative percentage of potential drop between the depletion layer and the Helmholtz layer.)

The onset of photocurrent will occur when the valence band edge reaches the electronic distribution curve of the electron donor in solution (Fig. 8a) so that tunneling across the interface will be possible. The photocurrent increases until the Fermi level and the value of the redox potential have nearly the same energy. At these conditions also a dark oxidation current is possible by electron injection into the conduction band (Fig. 8b). With further increase of dark current the actual concentration of donor ions at the surface is lowered with the consequence of decreasing the photocurrent (Fig. 8c).

5. Conclusions

In this work the photoelectrochemical behaviour of FeS_2 as an electrode material for a photocatalytic solar device has been investigated. But in spite of having the same crystal as well as electronic structure as RuS_2, the observed reactions in aqueous solutions are quite different: only a corrosion to SO_4^{2-} and no production of O_2 at positive potentials is observed. This difference can only be explained by higher catalytic activity of ruthenium caused by its different chemistry. But

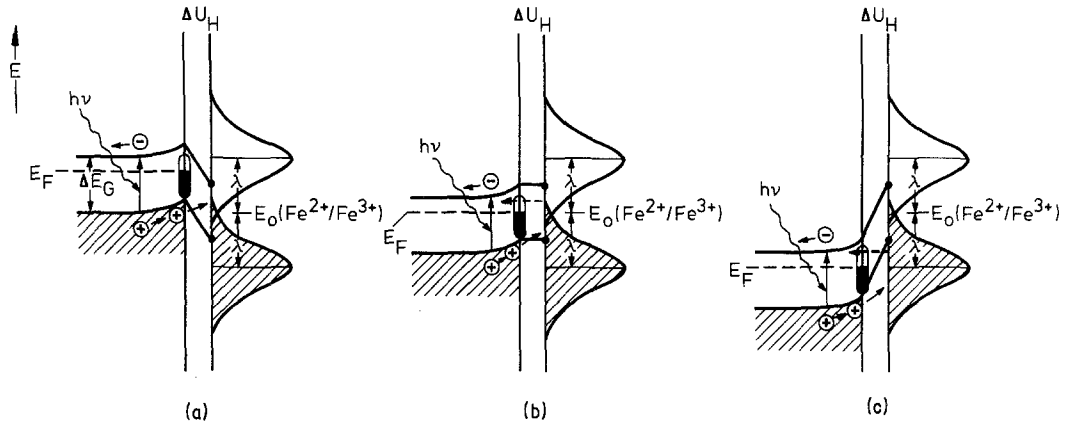

Fig. 8. Proposed energy scheme for the redox reactions at the FeS_2 surface. The Helmholtz layer is displayed larger for clarity. The interbandgap states are all represented as surface states. The band bending is assumed to be constant ($\lambda = 1.25$ V [33], $\Delta E_G = 0.9$ eV). (a) Onset of photocurrent (→). No dark current. (b) Maximum photocurrent (→). Small dark current (← –). (c) Small photocurrent (→). High dark current (← –).

for a detailed explanation the exact distribution of electronic states must be better understood.

Because of the high number of charge carriers present the natural pyrite specimen exhibit only small photocurrents. But in principle FeS_2 could be a promising material for solar energy converting devices as it is rather cheap and has a reasonably suitable energy bandgap of 0.9 eV. The Hall mobilities obtained were 100 $cm^2\ V^{-1}$ or less [32]. It can also be used as substrate material for depositing thin layers of semiconductors with metals of high catalytic activity crystallizing in the pyrite structure. Experiments of this type are performed in our laboratory.

There is also an interesting aspect to be mentioned in relation to geochemistry. The magnitude of photocurrents observed with natural pyrite indicates that photoelectrochemical mechanism should not be neglected in discussion of natural transformation and degradation of this abundant material.

Acknowledgements

The authors would like to thank Dr S. M. Ahmed for providing us with synthetic samples of FeS_2.

References

[1] H. Tributsch, *Struct. Bonding* 49 (1982) 127.
[2] L. F. Schneemeyer and M. S. Wrighton, *J. Amer. Chem. Soc.* 101 (1979) 6496.
[3] H. Tributsch and O. Gorochov, *Electrochim. Acta* 82 (1982) 45.
[4] H. Tributsch, *Z. Naturforsch.* 32a (1977) 972.
[5] R. Heindl, R. Parsons, A. M. Redon, H. Tributsch and J. Vigneron, *Surf. Sci.* 115 (1982) 91.
[6] H. Ezzaouia, R. Heindl, R. Parsons, and H. Tributsch, *J. Electroanal. Chem.* in press.
[7] G. Brostigen and A. Kjekshus, *Acta Chem. Scand.* 23 (1969) 2186.
[8] T. A. Bither, R. J. Bouchard, W. H. Cloud, P. C. Donohue and W. J. Siemons, *Inorg. Chem.* 7 (1968) 2208.
[9] R. Benoit, *J. Chem. Phys.* 52 (1955) 119.
[10] E. K. Li, K. H. Johnson, D. E. Eastman and J. L. Freeouf, *Phys. Rev. Lett.* 32 (1974) 470.
[11] D. W. Bullet, *J. Phys. C.* 15 (1982) 6163.
[12] H. van der Heide, R. Hemmel, C. F. van Bruggen and C. Haas, *J. Solid State Chem.* 33 (1980) 17.
[13] F. Hulliger, *Nature* 200 (1963) 1064.
[14] F. Hulliger and E. Mooser, *J. Phys. Chem. Solids* 26 (1965) 429.
[15] R. T. Shuey, 'Semiconducting Ore Minerals', Elsevier, London (1975).
[16] M. Pourbaix, 'Atlas d'Equilibres Electrochimiques', Gauthier-Villars et G., Paris (1963).
[17] G. Springer, *Inst. Mining Met. Trans. Sect. C* 79 (1970) C11.
[18] E. Peters and H. Majima, *Can. Met. Quart.* 7 (1969) 111.
[19] T. Biegler, D. A. J. Rand and R. Woods, *J. Electroanal. Chem.* 60 (1975) 151.
[20] T. Biegler, *ibid.* 70 (1976) 265.
[21] R. F. Meyer, *J. Electroanal. Chem.* 101 (1979) 59.
[22] A. Heller, B. Miller, H. J. Lewerenz, and K. J. Backmann, *J. Amer. Chem. Soc.* 102 (1980) 6555.
[23] F. A. Cotton and G. Wilkinson, 'Advanced Inorganic Chemistry', 3rd edn, Interscience Publishers, New York (1972).
[24] Sutarno, O. Knop and K. I. G. Reid, *Can. J. Chem.* 45 (1967) 1391.

[25] H. J. Lewerenz, S. Stucki and R. Kötz, *Surf. Sci.* in press.
[26] V. Ya. Shafirovich and V. V. Strelets, *Nouv. J. Chim.* **6** (1982) 183.
[27] Th. Carlson, 'Photoelectron and Auger Spectroscopy', Plenum Press, New York (1975).
[28] D. Briggs (ed.), 'Handbook of X-ray and Ultraviolet Photoelectron Spectroscopy', Heyden, London (1977).
[29] A. Müller, W. Jaegermann and J. H. Enemark, *Coord. Chem. Rev.* **46** (1982) 245.
[30] L. Vaska, *Acc. Chem. Res.* **9** (1976) 175.
[31] A. J. Bard, A. B. Bocarsly, F. -R. F. Fan, E. G. Walton and M. S. Wrighton, *J. Amer. Chem. Soc.* **102** (1980) 3671.
[32] J. C. Marinace, *Phys. Rev.* **96** (1954) 593.
[33] R. Memming and F. Möllers, *Ber. Bunsenges. Phys. Chem.* **76** (1976) 475.